Direct numerical simulations for drop impact on superhydrophobic patterned surfaces using the VoF method

Martina Baggio[1]*, Bernhard Weigand[1]
[1]Institute of Aerospace Thermodynamics, University of Stuttgart, Pfaffenwaldring 31, 70569 Stuttgart, Germany
*Corresponding author: martina.baggio@itlr.uni-stuttgart.de

Abstract
When considering drop impact on a superhydrophobic surface, it has been shown that drop rebound can occur faster on surfaces with millimetric-micrometric scale features in respect to flat surfaces. Numerous studies, mostly experimental, have dealt with the role of surface patterns in reducing the contact time between the solid surface and the liquid drop. On the other hand, only limited numerical work has been done on this topic, especially in conjunction with the Volume of Fluid (VoF) method. Since more than 20 years, the Institute of Aerospace Thermodynamics of the University of Stuttgart is developing its own, VoF-based program for direct numerical simulations (DNS) of multi-phase flows: Free Surface 3D (FS3D). Since FS3D is based on a Cartesian grid, we are currently implementing a method to represent the interaction of multi-phase flows with solid bodies embedded in a Cartesian geometry. In particular, we represent the embedded boundaries with an additional volume of fluid variable and, in each cell intersecting a boundary, we approximate the boundary surface with a plane (PLIC-scheme). We also deal with critical cells by merging them with one of their neighbors by means of a cell-linking strategy. In this work, we validate the method by comparing simulations of drop impact onto superhydrophobic featured walls with data from literature [2]. We simulate the case investigated by Chantelot et al. [2] of a water drop impacting on a superhydrobhobic surface with a spherical singularity. As in [2], we firstly study the drop impact at the top of the spherical singularity at different Weber numbers and then a set of simulations is carried out in which the centres of the drop and the sphere are horizontally shifted. We present the numerical setup, the grid and the used computational resources for each of our simulations. The results show a very good agreement for contact time and impact morphology, demonstrating the capability of FS3D in capturing the physics of the phenomenon.

Keywords
Direct numerical simulation, Volume of Fluid method, embedded boundaries, superhydrophobic surfaces.

Introduction

The role of millimetric-micrometric scale structures in changing the impact morphology of water droplets on superhydrophobic surfaces is of great interest in all those applications where the contact time between water drop and surface is of crucial importance, as for example for the anti-icing on airplane wings. Recently, numerous experimental studies have dealt with drop impact on different superhydrophobic structures; such as wires [3], ridges [9], and spherical singularities [2]. Chantelot et al. [2] also present numerical results obtained with the lattice Boltzmann method. Numerical studies about drop impact on superhydrophobic structured surfaces are however, to our knowledge, relatively rare. In this paper we present our study based on Free Surface 3D (FS3D), a CFD code for DNS simulations of multi-phase flows. FS3D has been developed at the Institute of Aerospace Thermodynamics at the University of Stuttgart and it has been in use since more than 20 years. This code can, between others, treat rigid particles immersed in a continuous fluid phase [8], but until recently could not handle different fluid phases interacting with arbitrary solid shapes. We are currently expanding FS3D to deal with this latter case. This work is organized as follows: in section "*Numerical Methods*" we briefly illustrate FS3D's numerical fundamentals and we discuss our method to treat solid boundaries embedded in a Cartesian grid. Secondly, in section "*Results and discussion*", we validate our method for the case studied by Chantelot et al. [2] for a water drop impacting onto a spherical singularity. Firstly we show our results for the centered impact on the top of the sphere at two different Weber numbers. Secondly, the case of off-centerd impact for three different offsets is studied. Also an overview of the numerical setup and used computational resources are given.

Numerical Methods

FS3D is a Cartesian, MAC-staggered [4] Finite Volumes code for DNS simulations of incompressible multi-phase flows. Multiple phases are handled with the VoF-Method [5]; that is, each phase i is represented by a color (step) function $\alpha_i(\boldsymbol{x})$, which is defined in each position $\boldsymbol{x} = x\boldsymbol{e}_1 + y\boldsymbol{e}_2 + z\boldsymbol{e}_3$ as follows:

$$\alpha_i(\boldsymbol{x}) = \begin{cases} 1 & \text{inside phase } i \\ 0 & \text{outside phase } i \end{cases} \tag{1}$$

Each material property of the flow $\phi(\boldsymbol{x})$ is assumed constant within each phase and can be described by the following formula:

$$\phi(\boldsymbol{x}) = \sum_{i=1}^{N_p-1} \alpha_i \phi_i(\boldsymbol{x}) + (1 - \sum_{i=1}^{N_p-1} \alpha_i(\boldsymbol{x}))\phi_{N_p} \tag{2}$$

where N_p is the number of phases, and where we used the fact that $\sum_{i=1}^{N_p} \alpha_i(\boldsymbol{x}) = 1$ in each position $\boldsymbol{x}$. The necessary equations for the temporal evolution of the interfaces between the phases are obtained by imposing the condition that the volume fraction $f_i = \left(\int_\Omega \alpha_i(\boldsymbol{x})\, d\Omega \right) / \Omega$ of each phase i is conserved in any arbitrary control volume Ω:

$$\frac{\partial f_i}{\partial t} = -\nabla \cdot (f \boldsymbol{u}) \quad i = 1, \ldots, N_p - 1 \tag{3}$$

where we assume that there is no phase change. After finite-volume discretization, f_i represents the volume fraction of the i-th phase in the considered computational cell. To avoid numerical diffusion, the PLIC-scheme [11] is used for sharp interface reconstruction: in each (scalar) control volume where $0 < f_i < 1$ the interface is reconstructed using a plane of orientation $\boldsymbol{n} = \nabla f_i$. In the following, we will only consider isothermal systems of a disperse liquid phase (water) immersed in a continuous gas phase (air) interacting with a fixed solid boundary. As a consequence, only the equation for the transport of the liquid volume fraction f is necessary for interface tracking. The remaining governing equations of our problem are the equation of mass conservation in incompressible flows:

$$\nabla \cdot \boldsymbol{u} = 0 \tag{4}$$

and the the Navier-Stokes equations for the transport of momentum:

$$\frac{\partial(\rho \boldsymbol{u})}{\partial t} + \nabla(\rho \boldsymbol{u} \otimes \boldsymbol{u}) = -\nabla p + \nabla \cdot \mathbb{S} + \rho \boldsymbol{g} + \mathbf{f}_\sigma \tag{5}$$

After time discretization, an equation for pressure is obtained by forcing the divergence-free condition on the velocity field:

$$\frac{\boldsymbol{u} - \tilde{\boldsymbol{u}}}{\Delta t} = -\frac{\nabla p}{\rho} \rightarrow \boldsymbol{u} = \tilde{\boldsymbol{u}} - \frac{\Delta t \nabla p}{\rho} \tag{6}$$

$$\nabla \cdot \boldsymbol{u} = \nabla \cdot \left(\tilde{\boldsymbol{u}} - \frac{\Delta t \nabla p}{\rho} \right) = 0 \rightarrow \nabla \cdot \left(\frac{\Delta t \nabla p}{\rho} \right) = \nabla \cdot \tilde{\boldsymbol{u}} \tag{7}$$

Where $\tilde{\boldsymbol{u}}$ is an intermediate velocity field to which all acceleration terms of equations 5, but the pressure term, have been added. Discretization of equation 7 leads to a linear system of equations for p which is dealt with a multigrid solver enmbedded into FS3D [12]. The final velocity field can then be obtained from 6.

Implementation of embedded boundaries

In this subsection our implementation of embedded boundaries is discussed briefly: a more detailed description can be found in [1]. The representation of rigid solid particles immersed in a continuous phase was implemented by Rauschenberger et al. [8] on the basis of the method developed by Patankar [6]. We base our work on this implementation: similarly to [8], embedded boundaries are described by their volume fraction f_b and the PLIC-scheme is used to represent their surface. Since there is no transmission of momentum from the fluid flow to the wall structures, we treat those as rigid bodies with infinite density. However, this causes the velocity grid nodes to be zero in all those (staggered) control volumes which contain a fraction of the boundary $f_b \neq 0$. Because the flow is incompressible, if the velocities are set to zero on $N_{faces} - 1$, then the velocity on the N_{faces}-th face also has to be zero (see figure 2). As a consequence, no advection of the fluid volume fraction f would be possible in those cells. Our solution consists in identifying critical cells (*slaves*) and merging them to their neighbor in the direction of the largest component of the boundary normal vector $\boldsymbol{n}_b$. This is possible by allocating *boundary cell* data structures in each boundary-crossed cell where $0 < f_b < 1$ and in their neighborhood (see figure 2). When a critical cell is

boundary cell	
`type(boundary cell), pointer:`	$master, slave$
`integer(1:3):`	$\boldsymbol{i} = i\boldsymbol{e}_1 + j\boldsymbol{e}_2 + k\boldsymbol{e}_3$

Figure 1. The structured data type `boundary cell`

identified, an univocal link between the master and its slave is established by means of the *master* and *slave* pointer attributes. This was possible because until now we only considered convex structures. However, an extension of our model allowing a master to have multiple slaves is possible. After *master-slave* linking, master and slave are

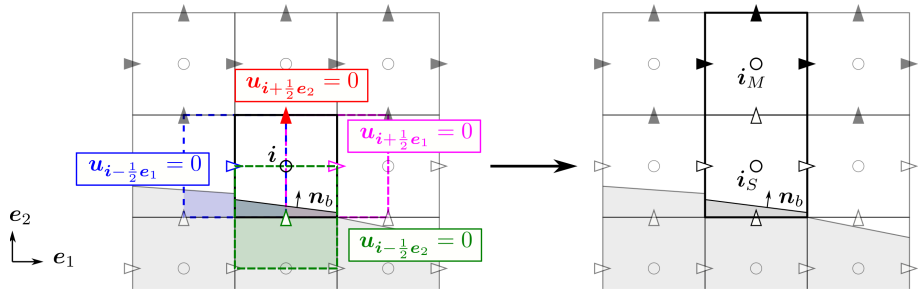

Figure 2. Left: a critical cell with zero velocities on all the faces. Right: *master-slave* linking.

treated as a single control volume. The advection of a fluid volume fraction is written in terms of the total volume fraction f_t in the master-slave cells. The adaptation of FS3D's original advection scheme [12, 11, 13]:

$$\frac{f_i^* - f_i^n}{\Delta t} = -\frac{F_{i+\frac{1}{2}e_1} - F_{i-\frac{1}{2}e_1}}{\Delta x_i} + [(1-\beta)f_i^n + \beta f_i^*]\frac{u_{i+\frac{1}{2}e_1} - u_{i-\frac{1}{2}e_1}}{\Delta x_i} \tag{8a}$$

$$\frac{f_i^{**} - f_i^*}{\Delta t} = -\frac{F_{i+\frac{1}{2}e_2} - F_{i-\frac{1}{2}e_2}}{\Delta y_i} + [(1-\beta)f_i^* + \beta f_i^{**}]\frac{v_{i+\frac{1}{2}e_2} - v_{i-\frac{1}{2}e_2}}{\Delta y_i} \tag{8b}$$

$$\frac{f_i^{n+1} - f_i^{**}}{\Delta t} = -\frac{F_{i+\frac{1}{2}e_3} - F_{i-\frac{1}{2}e_3}}{\Delta z_i} + [(1-\beta)f_i^{**} + \beta f_i^{n+1}]\frac{w_{i+\frac{1}{2}e_3} - w_{i-\frac{1}{2}e_3}}{\Delta z_i} \tag{8c}$$

takes then the following form for each step in any e_a advection direction:

$$\frac{f_t^* - f_t^n}{\Delta t} = -\frac{F_{OUT} - F_{IN}}{\Delta\Omega_{i_S} + \Delta\Omega_{i_M}} + [(1-\beta)f_t^n + \beta f_t^*]\frac{\dot{\Omega}_{OUT} - \dot{\Omega}_{IN}}{\Delta\Omega_{i_S} + \Delta\Omega_{i_M}} \tag{9}$$

where $\Delta\Omega_{i_{M,\,S}} = \Delta x_{i_{M,\,S}} \Delta y_{i_{M,\,S}} \Delta z_{i_{M,\,S}}$ are the volumes of the master and slave cells, $F_{OUT,\,IN}$ the volume fraction numerical fluxes across the master-slave faces in direction e_a, and $\dot{\Omega}_{OUT,\,IN}$ an altered divergence correction which takes the presence of the boundary into account (see figure 3). The numerical fluxes and the divergence cor-

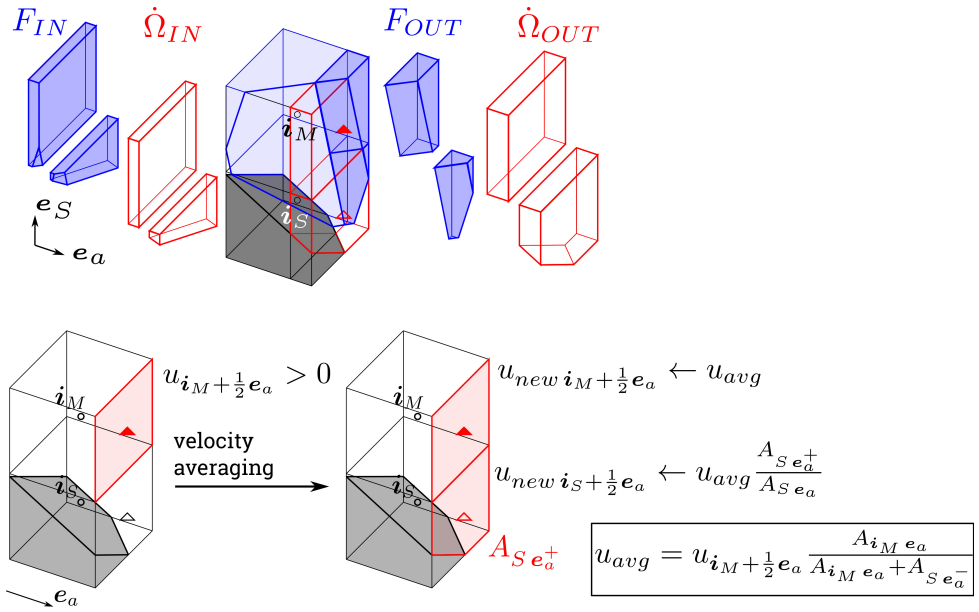

Figure 3. Top: volume fraction f_t advection on merged *master-slave* control volumes. Bottom: velocity averaging on the upwind faces of *master-slave* control volumes.

rection are calculated on the basis of an averaged velocity field on upwind faces of master-slave control volumes. The averaging procedure does not alter the product between velocity field and the lateral free faces of upwind master-slave control volumes. For example, at positions $i_M + (1/2)e_a$, $i_S + (1/2)e_a$:

$$u_{new\,i_M+\frac{1}{2}e_a} A_{i_M\,e_a} + u_{new\,i_S+\frac{1}{2}e_a} A_{i_S\,e_a} = u_{avg}(A_{i_M\,e_a} + A_{i_S\,e_a^+}) = A_{i_M\,e_a} u_{i_M+\frac{1}{2}e_a} \tag{10}$$

However, since the velocity field may be overwritten by neighbor cells, the divergence-free condition may be violated on master-slave control volumes and mass may not be conserved. In the simulations here presented, we observed that the error on mass conservation $E_{m\,max} = \|(m_t - m_0)/m_0\|_\infty$ was less than 0.5×10^{-5}, so negligible for the

case considered here. However, we are currently addressing this issue by extending our implementation towards a cut cell method similar to the one proposed by Popinet [7], with all the difficulties related to the implementation of this method on a staggered grid.

Results and discussion

In this paper, the impact of a water drop of radius R = 1.3 mm on a spherical feature of radius r = 0.2 mm is studied. This setup is analogous to the one of Chantelot et al. [2] and enables us to compare our results and assess the capabilities of our code. In particular, we investigate the following aspects:

1. Effect of impact velocity for centered impact.
2. Effect of an horizontal offset on contact time and impact morphology.

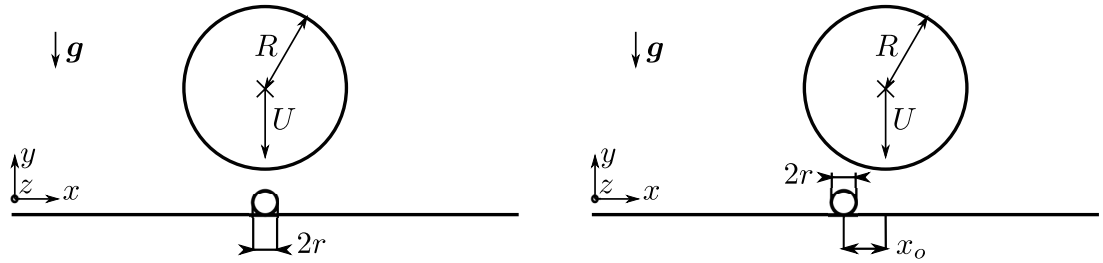

Figure 4. Setup of the considered case: a spherical drop of radius R = 1.3 mm impacting on a spherical feature of radius r = 0.2 mm without and with an horizontal offset x_o.

Centered impact at different velocites

Two different behaviours were observed in [2] for centered impacts. For low velocities, impact occurred as on a flat superhydrophobic surface. It has been shown that the contact time on a superhydrophobic flat surface is proportional to $\tau_0 \propto \sqrt{\rho R^3/\sigma}$ [10] and thus does not depend on the impact velocity. From their experiments, Richard et al. [10] estimated that $\tau_0 \approx 2.6\sqrt{\rho R^3/\sigma}$. As the velocity increases, the thickness of the lamella becomes comparable to the size of the sphere. As a consequence, the lamella ruptures and collides with the outer receding rim of the droplet, causing it to lift off with the shape of a torus. Because of the altered impact morphology, the contact time is remarkably reduced ($\tau \approx 1.24\sqrt{\rho R^3/\sigma}$ [2]). For R = 1.3 mm Chantelot et al. [2] determined the velocity threshold between the two regimes as U^* = 0.9 m s^{-1}. We considered two impact velocities: one under the threshold (U = 0.72 m s^{-1} < U^*) and one above (U = 1.28 m s^{-1} > U^*). Those velocities correspond to the Weber numbers $We = (\rho R U^2)/\sigma$ of 9.343 and 29.530 respectively. The simulations results at different times are shown in figure 5; it can be seen that FS3D successfully captures the expected impact morphology for both cases. In figure 6 the contact times of the simulations are plotted against the laws from literature for drop impact on a flat

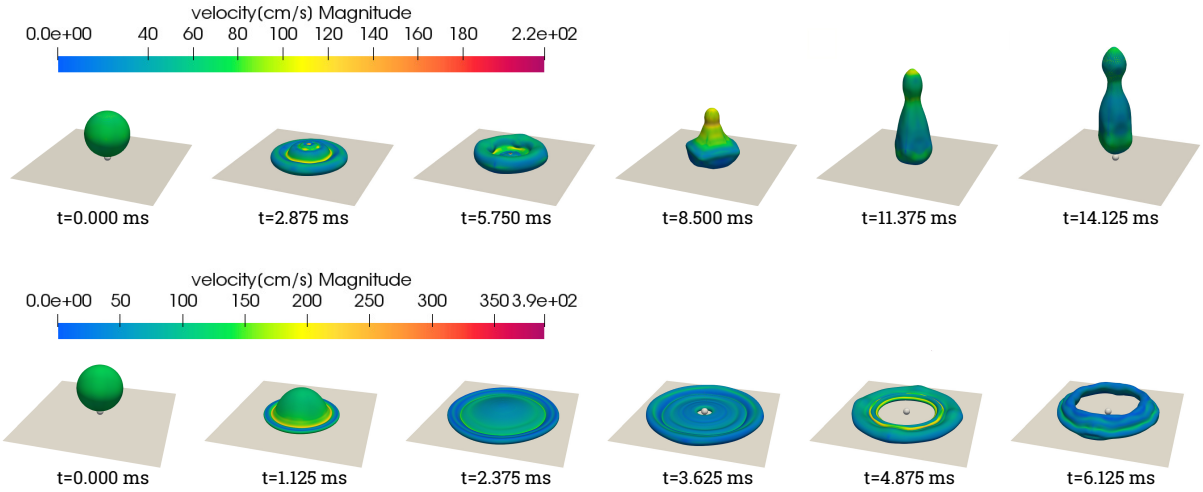

Figure 5. Results for centered impact of a spherical drop with radius R = 1.3 mm on a superhydrophobic surface with a spherical feature of radius r = 0.2 mm. Top: U = 0.72 m s^{-1}. Bottom: U = 1.28 m s^{-1}. For both cases, drop take off is shown in the last picture.

superhydrophobic surface ($\tau_0 = 2.6\sqrt{\rho R^3/\sigma}$ [10]) and for torus-shaped lift off ($\tau_0 = 1.24\sqrt{\rho R^3/\sigma}$ [2]). It can be seen that, although the contact time for the second case is slightly underestimated, the agreement with literature data is good.

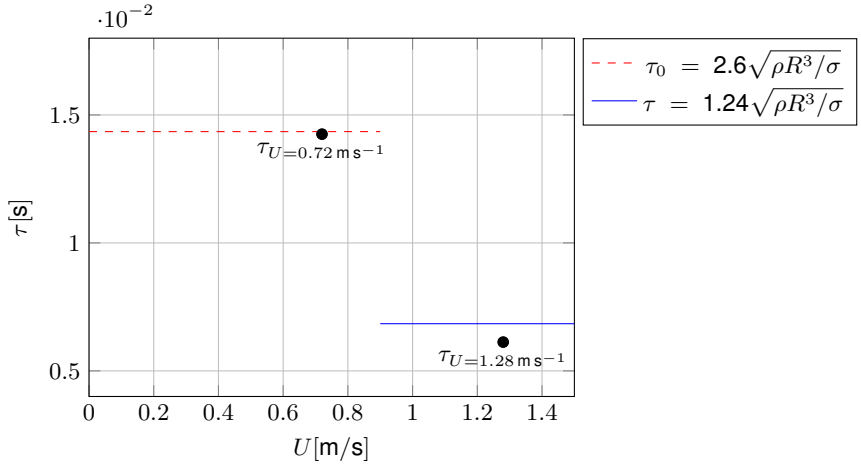

Figure 6. Contact time τ against impact velocity U for centered impact.

Off-centered impact

As observed by [10], the functional relation $\tau_0 \propto \sqrt{\rho R^3/\sigma}$ can be understood in terms of a balance between inertia ($\rho R/\tau^2$) and capillarity forces (σ/R^2). As the droplet size decreases, so does the contribution of the inertia force and detachment will occur more quickly. Chantelot et al. [2] deduce that the decrease in contact time for the ring-shaped take off is due to a change in characteristic length which they identify with the ring width l. For centered impact, $l \approx R_{max}$, where R_{max} is the maximum radius reached by the drop before recoil, and both sides of the ring bounce off symmetrically. They also show that, in presence of an horizontal offset x_o, the ring is characterized by two different widths $l^+ > R_{max}$ and $l^- < R_{max}$ and the two sides of the ring will leave the surface at different times with $\tau(l^-) < \tau(l^+)$. We carried out simulations for three different horizontal offsets (x_o = 0.25R, x_o = 0.50R, x_o = 0.75R) at the impact velocity of U = 1.28 m s^{-1} and estimated the characteristic lengths as $l^- = R_{max} - x_o$ and $l^+ = R_{max} + x_o$. The results for the temporal evolution of the impact are shown in figure 7. To compare our

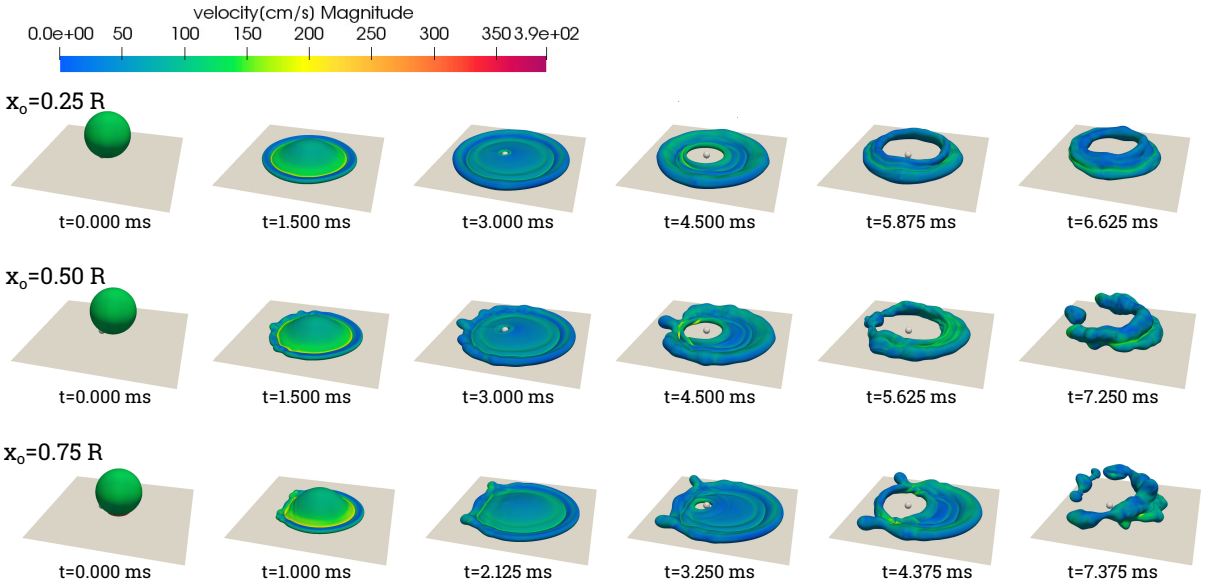

Figure 7. Drop impact for an horizontal offset of x_o = 0.25R (top), x_o = 0.50R (center), and x_o = 0.75R (bottom). The last two pictures of each set show the take off of the two sides of the ring.

results with the data from [2], the ratio of the contact time to the contact time for the flat case τ/τ_0 is plotted against the normalized characteristic length l/R_{max} in figure 8. The fit given by [2] for the contact time $\tau/\tau_0 \propto 0.37(l/R_{max})$ is also shown for comparison. It can bee seen that our data nicely follow the trend given by [2].

Numerical setup and computational cost

An overview of the numerical grid used for each simulation is shown in table 1. To reduce computational resources, only one quarter of the domain was simulated for centered impact and one half for the off-centered cases. The used boundary conditions were symmetry planes, no-slip for the wall and zero gradients for all remaining faces of the computational domain. The Cartesian mesh was refined on the solid sphere, so that its radius is resolved by

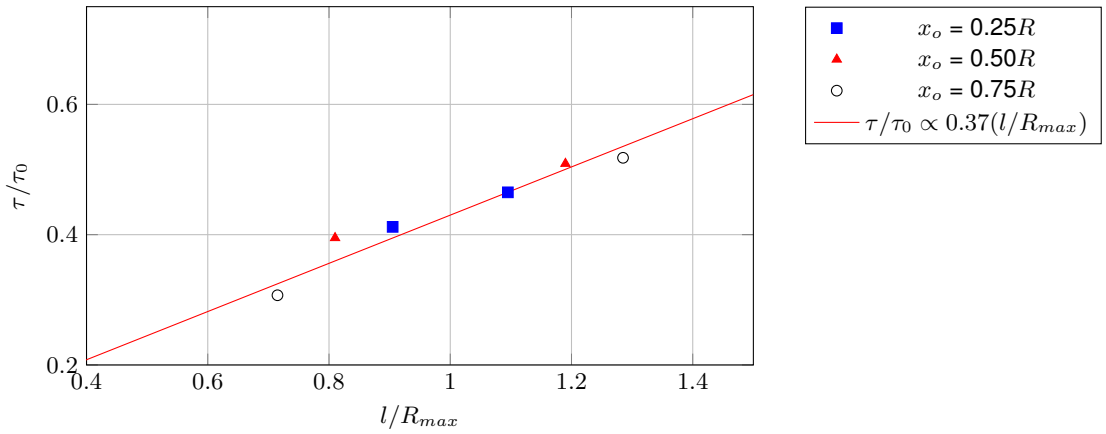

Figure 8. Normalized contact time τ/τ_0 against the normalized characteristic length of the ring l/R_{max} for off-centered impact.

about 60 grid cells. Here, a higher resolution would have been necessary to avoid the unphysical rupture of the film on the top of the sphere, which we observed in some cases (see figure 9). However, this would have resulted in a strong increase of the computational time. In addition, our simulations already show a very good agreement with experimental data. Table 1 also shows the used computational resources for each simulation. It can bee seen from the average number of cycles per second CPS that the current implementation is not very time efficient. However, this feature is still in the developing phase. In any case, no simulation took longer than four days.

Table 1. Used Computational resources for each simulation. From left to right: number of cell in each direction, number of used CPUs, average cycles per second, total number of cycles to lift off.

	$N_x \times N_y \times N_z$	N_{proc}	CPS [s^{-1}]	C_{tot}
Centered U = 1.28 m s^{-1}	384×384×384	144	0.2905	16362
Centered U = 0.72 m s^{-1}	384×512×384	288	0.1470	43731
Off-centered x_o=0.25R	768×384×384	288	0.1435	21074
Off-centered x_o=0.50R	768×384×384	288	0.1673	27790
Off-centered x_o=0.75R	768×384×384	288	0.2104	24457

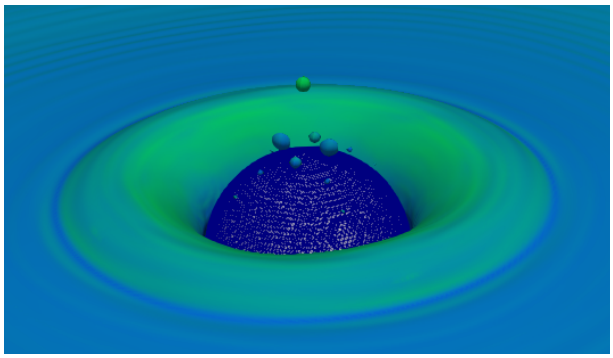

Figure 9. Unphysical breaking of the water film on the top of the sphere. The grid resolution of the spherical feature is also visible.

Conclusions

In this paper, we discussed our method to represent the interaction of multi-phase flows with complex solid boundaries in the Cartesian DNS code FS3D. The case of drop impact on a superhydrophobic wall with a spherical defect from [2] was simulated to compare the results with literature data. Different impact velocities and horizontal offsets were studied. The results show a generally very good agreement with the data from [2] in terms of contact time and impact morphology, proving the reliability of FS3D's predictions for this particular case. Further investigations with finer grids are under way.

Acknowledgements

We kindly thank the German Science Foundation (DFG) for its financial support within the International Research Training Group DROPIT (Droplet Interaction Technologies), GRK 2160/1.

Nomenclature

α	colour function
β	divergence correction parameter
ρ	density [kg m^{-3}]
σ	surface tension [kg s^{-1}]
τ	contact time [s]
ϕ	material property of the flow
Ω	volume [m^3]
A	area [m^2]
C_{tot}	total number of cycles to lift off
CPS	average number of cycles per second [s^{-1}]
$\boldsymbol{e}_{1,2,3}$	orthonormal basis of $\mathbb{R}^3$ and $\mathbb{Z}^3$
E_m	mass error
f	volume fraction
$\mathbf{f}_\sigma$	surface tension force per unit volume [N m^{-3}]
$\boldsymbol{i} = i\boldsymbol{e}_1 + j\boldsymbol{e}_2 + k\boldsymbol{e}_3$	cell index
l	characteristic size for torus-shaped take off [m]
M	master attribute of the data structure $\mathrm{boundary\ cell}$
m	mass [kg]
$\boldsymbol{n}$	normal vector [m^{-1}]
p	pressure [N m^{-2}]
R	drop radius [m]
$\mathbb{S}$	viscous stress tensor [N m^{-2}]
S	slave attribute of the data structure $\mathrm{boundary\ cell}$
r	radius of the spherical feature [m]
t	time [s]
U	impact velocity [m s^{-1}]
$\boldsymbol{u} = u\boldsymbol{e}_1 + v\boldsymbol{e}_2 + w\boldsymbol{e}_3$	velocity vector [m s^{-1}]
$\boldsymbol{x} = x\boldsymbol{e}_1 + y\boldsymbol{e}_2 + z\boldsymbol{e}_3$	space position [m]
x_o	horizontal offset [m]

References

[1] Baggio, M. and Weigand, B. “A numerical method for handling arbitrary solid boundaries within the DNS multiphase code Free Surface 3D (FS3D)”. In: ICLASS 2018, 14th Triennial International Conference on Liquid Atomization and Spray Systems. 2018.

[2] Chantelot, P., Moqaddam, A.M., Gauthier, A., S.S., Chikatamaria, C., Clante, and D., Quéré. “Water ring-bouncing on repellent singularities”. In: *Soft Matter* 14 (2018), pp. 2227–2233.

[3] Gauthier, A., Symon, S., Clanet, C., and Que´re´, D. “Water impacting on superhydrophobic macrotextures”. In: *Nature Communications* 6 (2015), p. 8001.

[4] Harlow, F.H. and Welch, J.E. “Numerical calculation of time-dependent viscous incompressible flow of fluid with free surface”. In: *The Physics of Fluids* 8.12 (1965), pp. 2182–2189.

[5] Hirt, C.W. and Nichols, B.D. “Volume of fluid (VOF) method for the dynamics of free boundaries”. In: *Journal of Computational Physics* 1.39 (1981), pp. 201–225.

[6] Patankar, N.A. “A formulation for fast computations of rigid particulate flows”. In: *Center for Turbulence Research, Annual Research Briefs* (2001), pp. 185–196.

[7] Popinet, S. “Gerris: a tree-based adaptive solver for the incompressible Euler equations in complex geometries”. In: *Journal of Computational Physics* 190 (2003), pp. 572–600.

[8] Rauschenberger, P. and Weigand, B. “Direct numerical simulation of rigid bodies in multiphase flow within an Eulerian framework”. In: *Journal of Computational Physics* 291 (2015), pp. 238–253.

[9] Regulagadda, K., Bakshi, S., and Das, S. K. “Morphology of drop impact on a superhydrophobic surface with macro-structures”. In: *Physics of fluids* 29 (8 2017), pp. 0821041–08210410.

[10] Richard, D., Clanet, C., and Quéré, D. “Contact time of a bouncing drop”. In: *nature* 417 (2002), pp. 811–812.

[11] Rider, W.J. and Kothe, D.B. “Reconstructing volume tracking”. In: *Journal of Computational Physics* 2.141 (1998), pp. 112–152.

[12] Rieber, M. “Numerische Modellierung der Dynamik freier Grenzflächen in Zweiphasenströmungen”. Doctoral thesis. University of Stuttgart, 2004.

[13] Strang, G. “On the construction and comparison of difference schemes”. In: *SIAM Journal of Numerical Analysis* 5.3 (1968), pp. 506–517.